A 3D glacier dynamics-line plume model to estimate the frontal ablation of Hansbreen, Svalbard

José M. Muñoz-Hermosilla[1], Jaime Otero[1], Eva De Andrés[1,2], Kaian Shahateet[1], Francisco Navarro[1], and Iván Pérez-Doña[1]

[1]Department of Mathematics applied to ICT, ETSI de Telecomunicación, Universidad Politécnica de Madrid, Spain
[2]Barcelona Expert Center, ICM-CSIC, Spain

Correspondence: José M. Muñoz-Hermosilla (jmmuhr@gmail.com)

Abstract. Frontal ablation is responsible for a large fraction of the mass loss from tidewater glaciers. The main contributors to frontal ablation are iceberg calving and submarine melting, with calving being the largest. However, submarine melting, in addition to its direct contribution to mass loss, also promotes calving through the changes induced in the stress field at the glacier terminus, so both processes should be jointly analysed. Among the factors influencing submarine melting, the formation
5 of a buoyant plume due to the emergence of fresh subglacial water at the glacier grounding line plays a key role. In this study we used Elmer/Ice to develop a 3D glacier dynamics model including calving and subglacial hydrology, coupled with a line-plume model to calculate the calving front position at every time-step. We applied this model to the Hansbreen–Hansbukta glacier–fjord system in Southern Spitsbergen, Svalbard, where a large set of data are available for both glacier and fjord, from September 2008 to March 2011. We found that our 3D model reproduced the expected seasonal cycle of advance-retreat.
10 Besides, the modelled front positions were in good agreement with the observed front positions at the central part of the calving front, with longitudinal differences, on average, below 15 meters for the period from December 2009 to March 2011. But there were regions of the front presenting major differences, specially the eastern margin.

1 Introduction

Svalbard is an Arctic region with a very high climatic sensitivity (Isaksen et al., 2016; Nordli et al., 2020). The ongoing climate
15 change context affects to the dynamics and mass balance of glaciers, and to the ocean's thermal and dynamical processes, leading to hydrological and ecological effects at regional and global scales, including sea level rise. Although the global glacier volume is only a small fraction of that of the Antarctic and Greenland ice sheets, glaciers currently lose more mass, and at similar or larger acceleration rates, than both sheets taken separately (Hugonnet et al., 2021). In fact, according to the Sixth Assessment Report of the IPCC Report of 2021 (IPCC, 2021), glaciers contribution to sea level rise has been very
20 significant for the period from 1971 to 2018 (22 % of the total estimation). The main reason is the high sensitivity of glaciers to atmospheric and oceanic forcing (Rignot et al., 2010; Motyka et al., 2013; Straneo and Cenedese, 2015; Luckman et al., 2015; Holmes et al., 2019). Mass change rate of Arctic glaciers, including Greenland's periphery, during the period from 2000 to 2018 ascends to -124.6 Gt a^{-1}, and represents a 46.7 % of the total rate for all the glaciers around the world (Hugonnet

et al., 2021). And frontal ablation of tidewater glaciers (mainly calving and submarine melting) represents between 10 and 30

25 % of this loss in regions such as Svalbard and the Russian Arctic (Huss and Hock, 2015; Hanna et al., 2020). Actually, among the seven Northern glacierized regions studied by Kochtitzky et al. (2022), the Russian Arctic experienced the highest frontal ablation rate during the period 2000-2020, followed by Svalbard.

The entire volume of water stored in Arctic glaciers, if melted completely, could rise sea level around 0.3 m (AMAP, 2017). The projections for this region through the 21st century show that its contribution will be significant (Meier et al., 2007; Church

30 et al., 2013; Hock et al., 2019) so, by the end of this period the estimated ice loss from glaciers would contribute between 3.9 and 9.2 cm to the sea level rise, around 56 % of the total glacier estimation (Edwards et al., 2021). In the case of Svalbard, the contribution to sea level rise is estimated between 0.75 and 1.25 cm (Edwards et al., 2021).

Tidewater glaciers are glaciers that terminate in the sea, with terminus either floating or grounded below the sea level (Cogley et al., 2011). The terminus position of these glaciers is an essential climate variable that helps to understand important processes

35 such as glacier mass balance or ice-ocean interactions (Bojinski et al., 2014). There have been many studies on the evolution of the front position of tidewater glaciers based on remote sensing data (e.g., at the local level, Błaszczyk et al. (2021)), but the relative importance of the various processes driving the front position changes remains poorly understood due to the scarcity of in-situ measurements. This scarcity is extreme in the case of basal conditions and subglacial hydrology. Besides, the zone close to the calving front is most often heavily crevassed, preventing measurements that could be useful to constrain processes such

40 as calving and submarine melting. Some recent works have started to cover this scarcity of direct measures with observations and the use of models regarding fjord water properties (Jackson et al., 2017, 2019), glacier front alterations (Vallot et al., 2019) or the whole glacier-fjord scheme (Cassotto et al., 2018; Jouvet et al., 2018; Sutherland et al., 2019; Xie et al., 2019). However, current understanding relies heavily on parameterizations of melting and entrainment, for which there is little in the way of validation (Hewitt, 2020). Summarizing, many features of tidewater glaciers still remain under-observed and poorly

45 characterised.

Computational models can help in understanding processes and predicting future evolution of glaciers. Yet, they require at least a minimum of observational input data. Moreover, the more realistic and complex models require a larger variety and amount of input data. In terms of calving, for example, the development of a simple calving law is still an unsolved problem (Benn et al., 2017; Benn and Åström, 2018). Therefore, it becomes necessary the use of computationally expensive 3D calving

50 models to reproduce the process with a fair degree of agreement to reality (Todd et al., 2018, 2019). In terms of submarine melting at tidewater glaciers, Jenkins (2011) implemented a one dimensional plume model by adapting his previous work (Jenkins, 1991) based on the theory of Morton et al. (1956), finding a relation between the subglacial runoff and the submarine melt rate. This model has been used to compute submarine melting in tidewater glaciers (Cownton et al., 2015, 2019; Slater et al., 2015, 2018). Cook et al. (2020, 2022) studied both calving and subglacial melting by coupling subglacial hydrology and

55 meltwater plumes to a 3D glacier dynamics model. These authors found significant results concerning the subglacial hydrology and its relationship with calving and plume processes, but they did not focus their work on the glacier terminus evolution. The front evolution, though, has been studied by some authors (Otero et al., 2017; De Andrés et al., 2018) using 2D models, evidencing the role of the back-pressure and the importance of oceanic and atmospheric processes. Even so, the lack of the

third dimension in the latter models prevented incorporating important dynamical 3D effects, such as lateral front melting. The two last-mentioned models were applied to the Hansbreen-Hansbutka glacier-fjord system, in Svalbard, which is our focus of interest, but there are not the only modelling works referred to this system. Oerlemans et al. (2011) proposed a minimal glacier model, in which the ice mechanics was strongly parameterised. The simple law for iceberg calving used in their model was able to match observed and simulated glacier length since 1900. Vieli et al. (2000, 2002) found that basal sliding processes strongly depend on the effective pressure and control the flow and the retreat of Hansbreen. Pętlicki et al. (2015), on the other hand, concluded that calving on Hansbreen is mainly triggered by the local imbalance of forces at the front, due to undercutting at the sea waterline and development of a thermo-erosional notch. More recently, De Andrés et al. (2021) made a comparison between a 2D glacier-fjord model and a 2D glacier-plume model regarding the calving front evolution. They determine that both models showed similar results for simulated glacier front positions under appropriate constraints of subglacial discharge, fjord temperature and crevasse water depth, but the glacier–plume model computational cost was significantly lower. Finally, Möller et al. (2023) presented a sensitivity study analysing the impact of five different bedrock datasets on projected mass losses from Hansbreen and suggested that under the influences of warmer climates accurate bedrock/ice thickness data are especially important for future glacier evolution modelling on decadal timescales.

In this work we aim to fill some of the above gaps by presenting a 3D full-Stokes Elmer/Ice-based ice flow model focused on Hansbreen's front evolution. To do so, we include atmospheric (through surface mass balance and surface meltwater), hydrological and oceanic processes (line-plume model), as well as a 3D calving law. We run the model for a total of 30 months, from September 2008 to March 2011, and analyse the model performance by comparing the monthly obtained front positions with observational data. By including all elements involved in frontal ablation this model is expected to be a valuable instrument to study the terminus evolution.

2 Data and methods

2.1 Study area

The glacier-fjord system Hansbreen-Hansbukta is located in one of the branches of Hornsund fjord in South West Spitsbergen, Svalbard, at $\sim$77ºN, $\sim$15.6ºE (Fig. 1). Hansbreen is a polythermal tidewater glacier flowing southward, that covers an area of $\sim$57 km^2. It is about 16 km long with a low mean surface slope of around 1.8° on average along the central flowline (Grabiec et al., 2012). Its calving front is 1.5 km wide with a vertical face $\sim$100 m thick at the central flowline, of which 50 to 60 m are below the sea level. The seasonal retreat of Hansbreen usually starts in June/July and lasts until late autumn/early winter, and the average summer and winter fluctuations amount to -125 and 79 m, respectively (Błaszczyk et al., 2021). As for Hansbukta, it is a $\sim$2 km long bay, with maximum depth of $\sim$77 m. Temperature and salinity in Hansbukta experiences strong seasonal variability, ranging from -1.8 to 3°C and from 34.6 to 31.8 PSU between April and August, respectively.
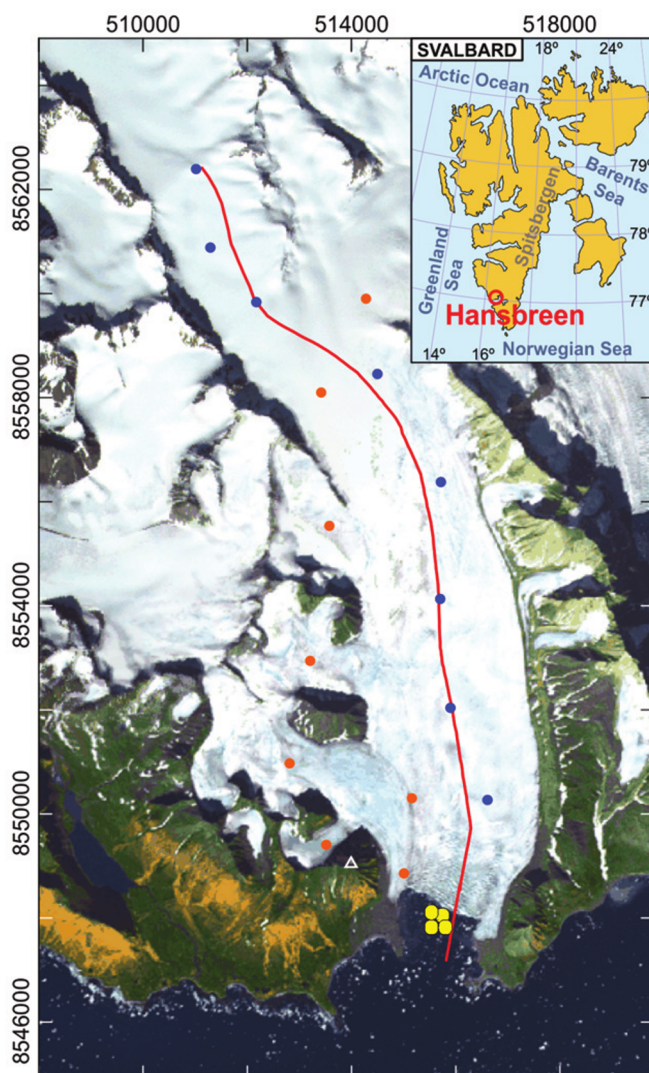
Figure 1. Location of Hansbreen–Hansbukta, Svalbard (inset). ASTER image of Hansbreen–Hansbukta showing the location of the stakes for velocity measurements (blue circles for the flowline and red circles for the rest of the stakes) and the conductivity–temperature–depth (CTD) profiles in Hansbukta (yellow circles) (De Andrés et al., 2021). The white triangle indicates the position of the time-lapse camera. The axes include the UTM coordinates (m) for zone 33X.

2.1.1 Data

90 The model uses as input gridded surface velocity data. The ice surface velocities were obtained by applying Bayesian Kriging (BK) techniques (Perez-Doña and Otero, 2023) (Fig. 2) on daily horizontal velocities measured between May 2005 and April 2011 at a set of stakes located along the glacier. As a prior for the BK, a distribution of the surface velocity module of Hansbreen
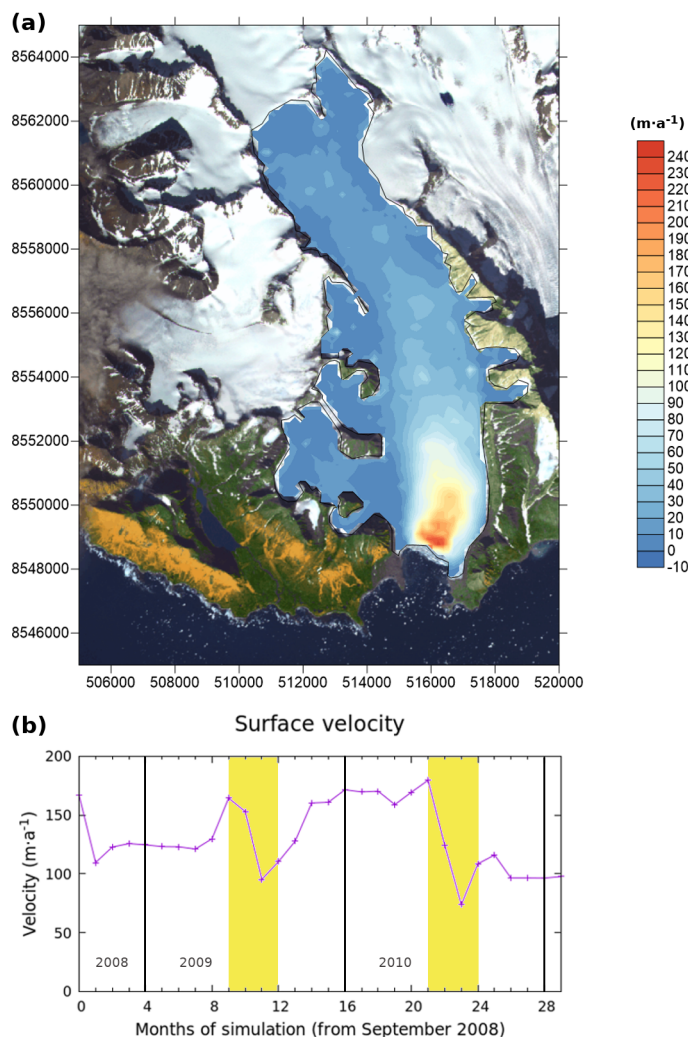
Figure 2. (a) Hansbreen's surface velocity distribution obtained from BK algorithm corresponding to September 2008, and (b) time evolution of the velocity at the stake located closer to the calving front (the southernmost blue point in Fig. 1). The yellow areas in the graph indicate the summer periods (June to September 2009 and 2010) and the black vertical lines separate the different years. The satellite image used as background was available from ASTER © METI and NASA, all rights reserved, courtesy of the University of Silesia, Poland, within the frame of cooperation of the SvalGlac project.

was calculated as the averaged velocities derived from measurements taken by TerraSAR-X from January 2013 to August 2014 using feature tracking (Adrian Luckman, personal communication).

95   Front position data from time-lapse camera images taken every 3 hours were processed and averaged over weekly intervals between December 2009 and September 2011 (Otero et al., 2017). Surface mass balance (SMB) and surface meltwater (SMW) were obtained from downscaled European Arctic Reanalysis data at 2 km horizontal and hourly temporal resolutions,

constrained by automatic weather stations and stake observations (Finkelnburg, 2013). The surface elevation came from the SPIRIT digital elevation model for gentle slopes, with a 30 m RMS absolute horizontal precision and 40 m resolution. Bedrock

100 topography was inferred from ground-penetrating radar data (Grabiec et al., 2012; Navarro et al., 2014).

Hydrographic data consist of a set of CTD casts (i.e., conductivity, temperature and depth profiles) in Hansbukta (yellow points in Fig. 1). All the data were vertically averaged every 1 dbar (1 kPa). Available CTD oceanographic data only covered the period from April 2010 to August 2010, with a long gap between April and July. Linear interpolation was used to fill in the period from April 2010 to July 2010. Since mooring data indicate that the temperature and salinity records remained

105 relatively stable between November and April (De Andrés et al., 2018, Supp Info.), a linear extrapolation was used to estimate temperature and salinity from August to November. The values for November (winter conditions) were extended until March.

2.2 Model

We use the open-source, full-Stokes, finite element, ice flow model Elmer/Ice (Gagliardini et al., 2013) including the GlaDS hydrological model (Werder et al., 2013), the free surface evolution, a 3D calving module (Todd et al., 2018) and a continuous

110 sheet-style 'line' plume across the width of the calving front (Cook et al., 2020) to study Hansbreen's front evolution from September 2008 to March 2011. We follow the work of Cook et al. (2022), but with an asynchronous coupling between the subglacial hydrology and the ice flow (and the calving and the plume), i.e., the subglacial hydrology that generates the plume is computed monthly whereas the time-step of the ice-flow simulation is one day.

2.2.1 Ice-flow model

115 The horizontal mesh is composed of triangles and it has been designed to have a maximum resolution of 50 m at the calving front. The resolution decreases progressively upglacier, reaching 200 m at 5 km from the front. Beyond that, the mesh continues coarsening to get to 500 m at the head of the glacier. This horizontal mesh is then vertically extruded on 10 levels, resulting in a 3D mesh composed of triangular prisms. The model solves the full-Stokes equations for ice flow, with rheology defined by Glen's flow law (e.g., Cuffey and Paterson, 2010) and uses the calving implementation described by Todd et al. (2018, 2019)

120 and Cook et al. (2020, 2022), following Otero et al. (2010) and Todd and Christoffersen (2014). This implementation is an improved formulation of the crevasse depth calving criterion postulated by Benn et al. (2007) and Nick et al. (2010) for use in a 3D framework. Crevasse depths are, therefore, calculated following:

$$\sigma_n = 2\tau_e sgn(\tau_{xx}) - \rho_i g d + P_w \tag{1}$$

where σ_n is the net stress (positive for extension and negative for compression). The terms on the right-hand side represents the

125 balance of forces: the first corresponds to the opening force of longitudinal stretching, where τ_e represents the effective stress, $\tau_e^2 = \tau_{xx}^2 + \tau_{zx}^2$ and the sign function ensures that crevasses opening is only produced under longitudinal extension; the second term corresponds to the ice overburden pressure, which leads to creep closure, where ρ_i is the ice density, g is the acceleration of gravity and d stands for the crevasses depth. P_w stands for the water pressure which contributes to open the crevasses. This term is here considered to be zero for surface crevasses because they are capable of opening without water pressure. For basal

130   crevasses, on the other hand, water pressure is controlled by the subglacial hydrological system and at the calving front can be expressed as:

$$P_w = (Z_{sl} - Z)\rho_w g \qquad (2)$$

being ρ_w the density of water at the calving front and Z the elevation with respect to sea level. Z_{sl} denotes the sea level and is set to 0 m. This improved criterion specifies calving to occur either when surface crevasses reach the waterline or when surface

135   and basal crevasses meet.

2.2.2   Boundary conditions

At the head of the glacier, the ice divide, horizontal velocities and shear stresses are set to zero. No flow is allowed through the lateral margins of the glacier, where no-slip conditions are additionally imposed. The upper free surface is constrained to a surface mass-balance accumulation flux boundary condition (positive for accumulation, negative for ablation). This flux is

140   obtained by calculating monthly means of the SMB data described in the Data section. A simple Weertman-type sliding law is applied at the base following:

$$\tau_b = \beta u_b \qquad (3)$$

where τ_b is the basal stress, u_b is the basal velocity and β is the slip coefficient. We use inverse methods to determine β (Gillet-Chaulet et al., 2012). A hydrostatic sea-water pressure condition is also imposed at the submerged part of the glacier front.

145   Hansbreen's front is considered a near-vertical front, which simplifies the domain geometry of our model.

2.2.3   Subglacial hydrology

We use the GladS module of Elmer/Ice (Gagliardini and Werder, 2018) to model Hansbreen's subglacial hydrology. Glads (Glacier Drainage System) simulates both inefficient distributed drainage, represented by a sheet of water that covers the whole area of the glacier, and efficient channelised drainage, represented by a series of channels generated on the edges of the

150   mesh elements of the domain (See more detail in Werder et al. (2013)). The implementation of the hydrological model for this work has been adapted, regarding the size of our domain, following Gagliardini and Werder (2018) and Cook et al. (2020). The main parameters of the model are set out in Table 1.

    We use GladS to obtain subglacial discharge estimates at the grounding line. Therefore, it is run at the bed of the glacier using the same mesh as the ice model to avoid complexity. Water is not permitted to flow through the lateral boundaries and

155   we set the hydraulic potential, ϕ, to zero at the grounding line. This follows from equation (2) combined with the definition of the hydraulic potential:

$$\phi = \rho_w g Z + P_w \qquad (4)$$

Water entering the hydrological system is derived from surface and basal meltwater production. Surface melting is determined by calculating monthly averages for the surface meltwater, assuming it travels directly to the bed at the same point of production

Table 1. Parameters used for GlaDS model in this study

Description	Name	Value	Units
Pressure melt coefficient	c_t	$7.5 \cdot 10^{-8}$	KPa^{-1}
Heat capacity of water	c_w	4220	$\mathrm{J\,kg^{-1}K^{-1}}$
Sheet flow exponent	α_s	3	
Sheet flow exponent	β_s	2	
Channel flow exponent	α_c	5/4	
Channel flow exponent	β_c	3/2	
Sheet conductivity	k_s	0.005	$\mathrm{m\,s^{-1}kg^{-1}}$
Channel conductivity	k_c	0.1	$\mathrm{m^{3/2}kg^{-1/2}}$
Sheet width below chann	l_c	0.2	m
Cavity spacing	l_r	0.5	m
Bedrock bump ratio	h_r	0.02	m
Englacial void ratio	e_v	10^{-4}	

160   at the surface. As for basal meltwater, we suppose a distributed melt calculated using a geothermal heat flux of 63 mW m^{-2} (Gagliardini and Werder, 2018).

2.2.4   Plume model

In this work we use a plume model implemented in Elmer/Ice (Cook et al., 2020, 2022) based on buoyant plume theory (Jenkins, 2011; Slater et al., 2015). In that model, a continuous sheet-style 'line' plume, split into coterminous segments, is
165   simulated across the calving front. The field studies carried out on tidewater glaciers (Fried et al., 2015; Jackson et al., 2017) justify the election of this plume geometry.

The plume model is initialised by the subglacial discharge at each node of the grounding-line, where the subglacial discharge values are obtained as solution of the subglacial hydrology model. Due to the density differences between meltwater and fjord water, subglacial discharge water rises in contact with the calving front mixing turbulently with the surrounding water
170   and producing melting at the ice–water interface. The calculated melt rates are then applied to modify the geometry of the submerged part of the calving front.

2.2.5   Model design

This model is implemented in monthly cycles that are run sequentially to cover the total simulation time, September 2008-March 2011. Every cycle is divided into 3 steps (Fig. 3):

175   1. Inversion for slip coefficient: an inversion using adjoint methods (Gillet-Chaulet et al., 2012) is performed to adjust the slip coefficient to the changing mean velocities for a given month. This is done by minimizing a cost function for the

velocities, running monthly steady-state simulations. It is done monthly to account for the changes in the velocity field while keeping a reasonable computational cost.

2. Dynamical and hydrological models, and free surface evolution: from the inversion results, a 30-day transient simulation is run with a 1-day time-step, where the glacier surface is left to evolve freely. Subsequently, the daily subglacial discharge values are averaged over the month.

3. Calving and plume models: the monthly-averaged values of subglacial discharge and the fjord ambient conditions are the required input for the line-plume model. The dynamic model is run again for a month with a 1-day time-step, but now with the modules for calving and plume enabled. Consequently, the front is allowed to evolve as a combination of ice-flow and calving, while submarine melting changes the submerged geometry of the calving front. Therefore, each of these time steps results in a new glacier geometry and a new front position.

The first cycle starts from the geometry described in Sect. 2.1, while every new cycle will start from the resulting geometry of the previous one.

3 Results

Starting in September 2008, the modelled monthly values of surface meltwater, subglacial discharge, plume melt rate and number of calving events present a seasonal pattern (Fig. 4). The largest SMW values are reached in July (8.9×10^5 m^3 a^{-1} and 8.3×10^5 m^3 a^{-1} for 2009 and 2010 respectively), and the cumulative SMW for both summer seasons is of the same order of magnitude, being the value for 2010 $\sim$6 % lower than the one for 2009 (Fig. 4(a)). The largest subglacial discharge values are also reached in July (9.1×10^5 m^3 a^{-1} and 5.7×10^5 m^3 a^{-1} for 2009 and 2010 respectively), but the total amount for both summer seasons varies significantly, by $\sim$25 % (Fig. 4(b)). Beyond the summer months, SMW and subglacial discharge maintain a baseline value around 1×10^5 m^3 a^{-1}.

The total melt rate due to plume activity presents a difference of $\sim$6 % between the two summer periods (1.7×10^5 m^3 a^{-1} and 1.6×10^5 m^3 a^{-1} for 2009 and 2010 respectively). The largest plume melt rates for each summer period are reached in different months, August for 2009 (7.1×10^4 m^3 a^{-1}) and July for 2010 (5.9×10^4 m^3 a^{-1}) (Fig. 4(c)). Other than that, June presents values around 2.6×10^4 m^3 a^{-1} and September around 1.3×10^4 m^3 a^{-1}. Note that no plume melt rate is produced from November to April, as no plumes are formed during these months.

The number of calving events reaches the highest values in summer, being August the month with the largest number of events in both years (127 in 2009 and 138 in 2010) (Fig. 4(d)). The simulation starts in September 2008 and presents a value (90) significantly higher than the following Septembers. The patterns for summers 2009 and 2010 show dissimilarities: in summer 2009, August concentrates almost the total number of events for the period, far followed by September (less than half), and with very small values in July and October. By contrast, in summer 2010, even if August accounts for the highest value too, the calving events distribution is totally different, since a large number of them take place in July. Moreover, September and October present values of the same order, both of them larger than the previous September. In one third of the months that
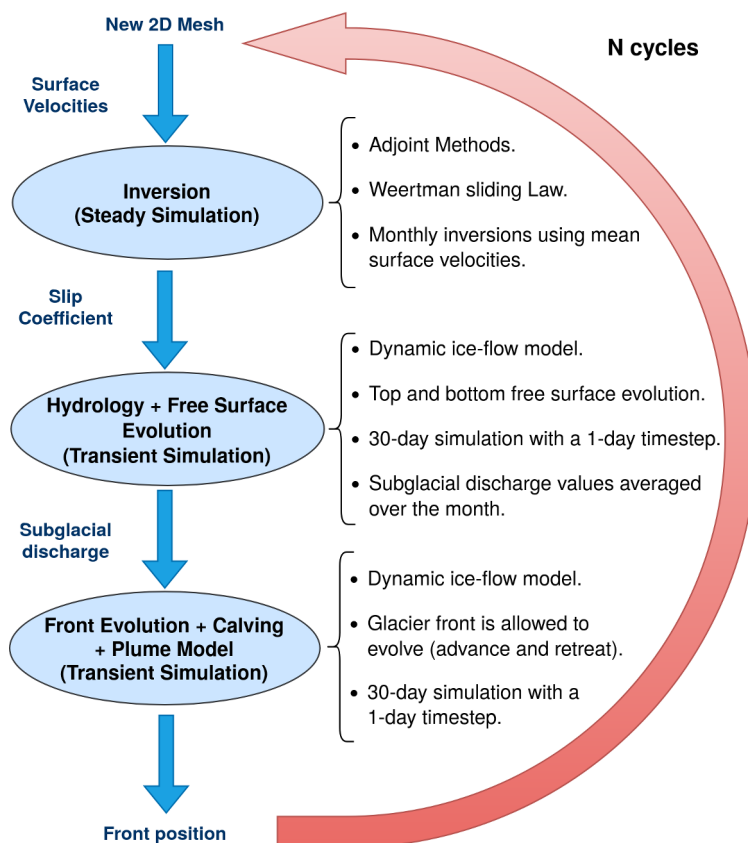
Figure 3. Schematics of the 3-step model procedure: inversion, dynamic model with hydrology module, and dynamic model with calving and plume modules. The red arrow indicates that a series of N cycles are run to cover the total simulation period.

comprise the simulation, the number of calving event is zero, and almost in another third is less than 5. In general, the lowest

210   values correspond to the winter months, but showing different patterns: the periods November 2008-June 2009, November 2009-June 2010 and November 2010-March 2011 exhibit calving events occurring at different rates and number.

The calving front follows a seasonal pattern in terms of advance and retreat along the whole simulation period, generally retreating in summer and advancing during the rest of the year (Fig. 5). The periods of advance are longer and the advancing rate moves from 10 m mo^{-1} to 20 m mo^{-1} of longitudinal difference, calculated as the difference in area between subsequent

215   months divided by the glacier width. On the other hand, the periods of retreat are shorter and the retreating rate can reach up to -30 m mo^{-1}. The largest negative values (indicating retreat) occur at the beginning of the simulation (September and October 2008) and, beyond that, in August 2009 and 2010. The total advance is larger in the first advance period (November 2008-July 2009), 124.59 m mo^{-1}, than in the second one (October 2009-June 2010), 108.45 m mo^{-1}. As for cumulative retreat, in the first period (August 2009-September 2009) amounts to -33.94 m mo^{-1}, whereas in the second one (July 2010-November 2010)

220   is -38.23 m mo^{-1}. The cumulative retreat reaches its highest value, of -61.59 m mo^{-1}, in the two first months of the simulation.
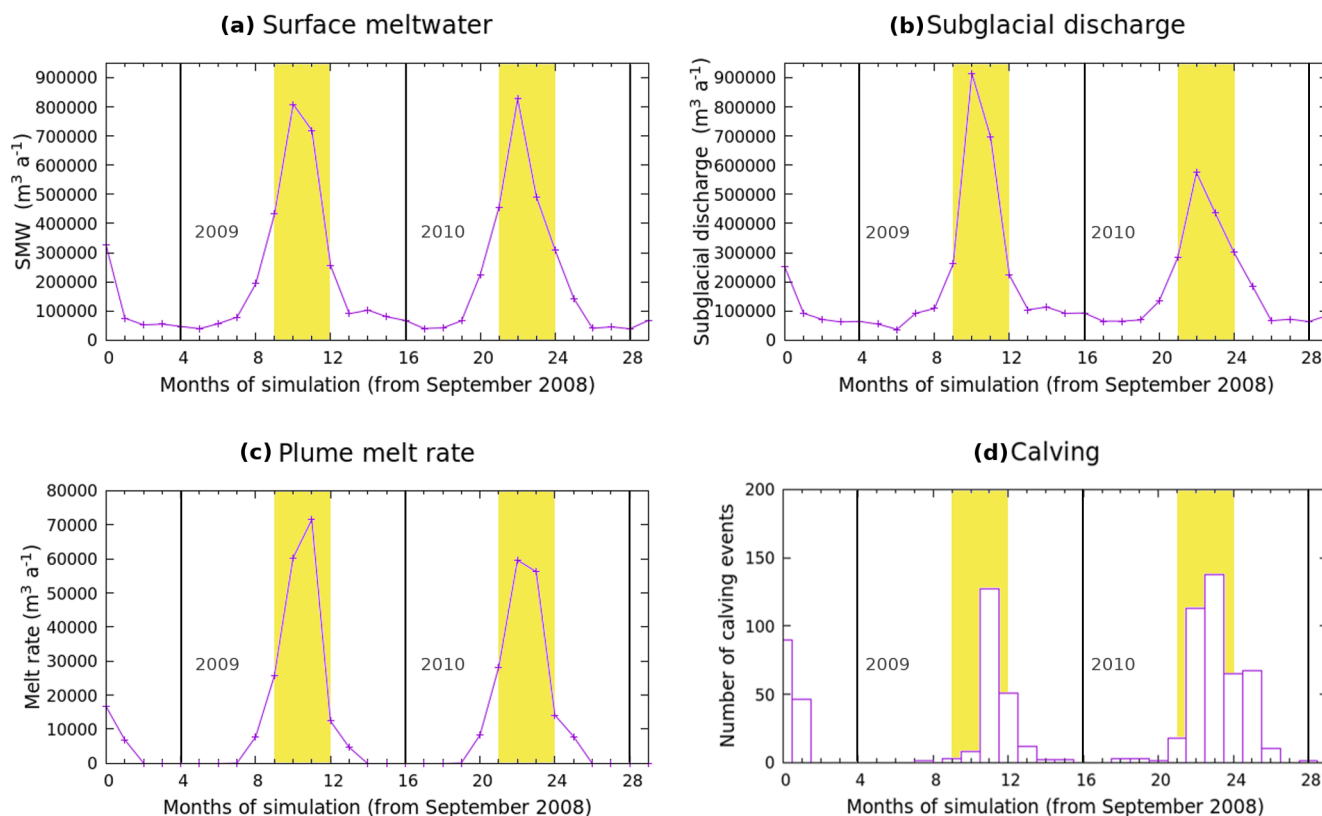
Figure 4. Temporal evolution of: (a) surface meltwater (SMW), (b) subglacial discharge produced by surface and basal melt for every month of the simulation, (c) total melt rate produced by plume activity computed on the first day of every month of the simulation and (d) the number of calving events produced by the model at every month of the simulation. The yellow areas indicate the summer periods (June to September 2009 and 2010) and the black vertical lines separate the different years.

By the end of the first year of simulation, September 2009, the front position has advanced 29.05 m mo^{-1} with respect to the position in September 2008, while by the end of the second year of simulation, September 2010, the front position has advanced 73.38 m mo^{-1} with respect to September 2009, resulting in a total advance of 102.43 m mo^{-1} with respect to September 2008. The map in Fig. 5 shows some front positions.

4   Discussion

The results of the model indicate that the glacier presents a marked seasonal behaviour. Figures 2 and 4(a) exemplify this feature in the input data as well. Subglacial discarge values correlate with surface meltwater values (Fig. 4(a), (b)). It has been applied a constant value of basal and internal melting ($\sim 2.6 \times 10^4$ m^3 a^{-1}) by using the geothermal heat flux defined in Sect. 2.2.3, which explains, as well as some other processes like internal refreezing, why in some months the subglacial discharge is
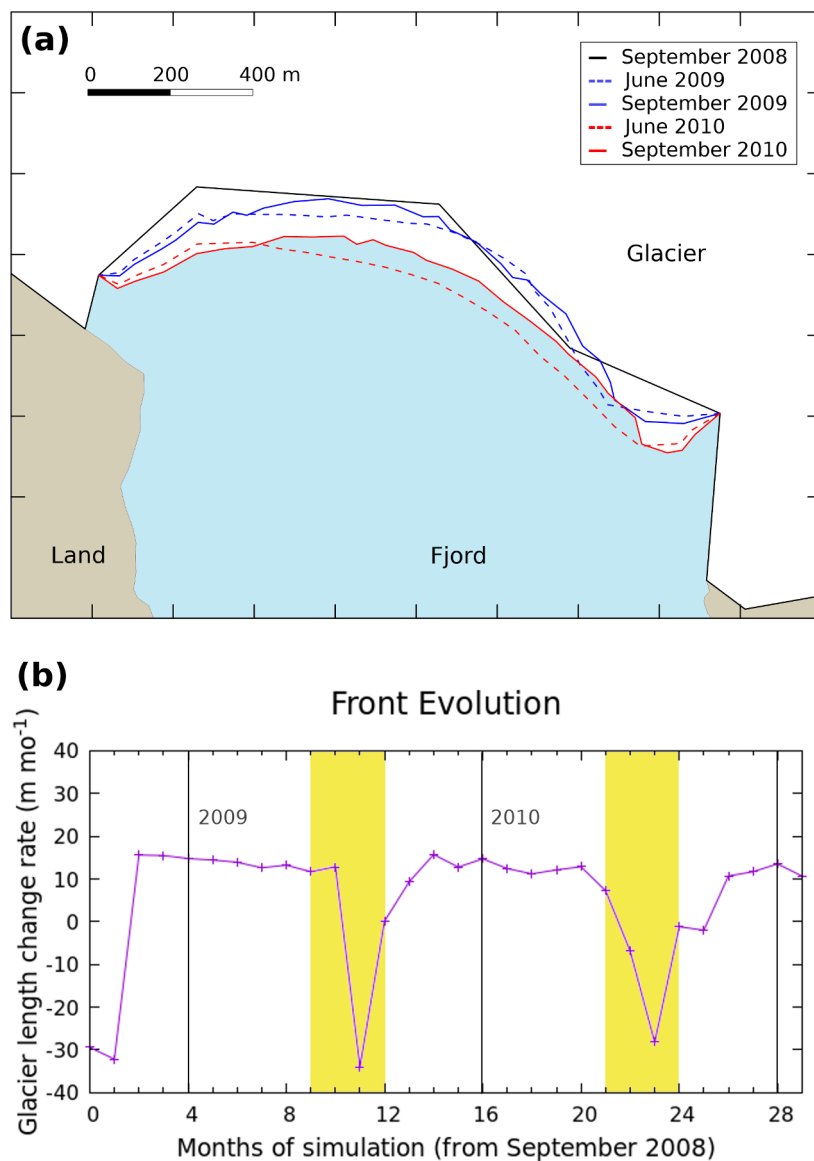
The Cryosphere
Discussions

Open Access

EGU

(a)

(b)

Front Evolution

Figure 5. Calving front evolution during the simulation. In (a), some front position are printed in different colours: the solid lines correspond to September 2008 (black), September 2009 (blue) and September 2010 (red), whereas the dashed lines correspond to June 2009 (blue) and June 2010 (red). The graph (b) represents the longitudinal difference along the whole simulation, calculated as the difference in area between subsequent months divided by the glacier width. The yellow areas indicate the summer periods (June to September 2009 and 2010) and the black vertical lines separate the different years.

230   larger than the SMW. A 6 % decrease in SMW in summer 2010 was responsible for the 25 % decrease in subglacial discharge
for the same period. However, this reduction in subglacial discharge cannot be fully attributed to the decrease in SMW. One
possible explanation for this subglacial discharge reduction is a change in the efficiency of the drainage system that is not being
captured by the model. This change would be consistent with the marked decrease in the velocity values at the beginning of
summer 2010 (Fig. 2).

235   Now, plume melt rate is affected by both fjord ambient conditions and subglacial discharge. The model calculates non-zero
freshwater flux into the fjord in winter months (Fig. 4(b)), in agreement with Cook et al. (2020). However, in the present study,
either the subglacial discharge values are not high enough or the winter ambient conditions are not suitable for the occurrence
of plumes, unlike the work of Cook et al. (2020) (Fig. 4(c)). On the other hand, between April and October, both ambient
conditions and subglacial discharge values are suitable for the occurrence of plumes. The ambient conditions in the fjord were

240   kept the same for both summer periods. Hence, the differences between the them can be explained by the differences in the
subglacial discharge that feeds the plumes. As an exemplification, Fig. 6 shows two different distributions of the plume melt
rate at the calving front: a high-melting month, August 2009 (a) and a low-melting month, October 2009 (b). The plume melt
rate in August 2009 is not only higher than the plume melt rate in October 2009, but it also extends to a larger area of the
calving front. Comparing with other authors working on the same glacier-fjord system, the maximum melt rate values obtained

245   for August 2010 are consistent with the ones obtained by De Andrés et al. (2018) (58 m^3 mo^{-1} versus 15 m^3 week^{-1}).

As for the calving, the events produced in the summer of 2010 almost double the value for 2009 (334 versus 189) and, in
fact, extending the period until October, it is exactly the double (401 versus 201). This difference in the number of events
explains why the absolute value of the retreat is larger in 2010 than in 2009, as can be observed in Fig. 5. The larger number
of events obtained in September 2010 and October 2010 in comparison with the same months in 2009 can be favoured for the

250   larger values of plume melt rate.

To study the behavior of the calving front and how it compares to the expected behavior of a tidewater glacier, Fig. 5 outputs
some interesting features. First of all, the glacier advances steadily during the winter months, when calving is not present
in general, and retreats during the summer months, specially in August, when it reaches the highest absolute values. So, in
general, the model is able to reproduce the seasonal tidewater glacier cycle. Secondly, calving is the main contributor to frontal

255   ablation, but plume-induced melt can lead to a larger number of calving events, so both factors are important in the control of
the front position. Finally, the glacier front remains quite stable during the study period. In fact, it experiments a small advance
between September 2008 and 2010, in agreement with Błaszczyk et al. (2021).

To validate the model performance, we compare the modelled and observed front positions (Fig. 7). The modelled positions
are in general more advanced than the observed ones. The difference between modelled and observed positions varies through-

260   out the simulation. It starts by a decreasing period from December 2009 to July 2010. Afterwards, there is an increasing period
from August 2010 to November 2010, followed by a final decrease until the end of the simulation in March 2011 (Fig. 8).
There seems to be a seasonal pattern, but the lack of data beyond March 2011 do not allow us to establish such a thing. The
results present a marked contrast between the central part and the east lateral margin of the glacier front, so that the maximum
differences in the eastern zone of the front are approximately 10 times larger than in the central one. This is likely due to the
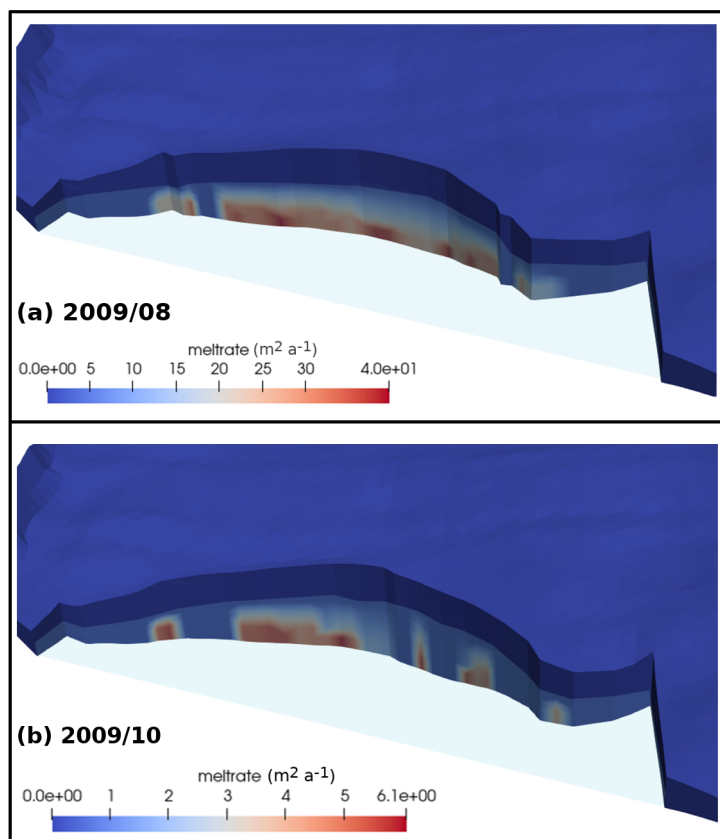
Figure 6. 3D aerial view of the glacier calving front for (a) August 2009 and (b) October 2009. The red zones represent high values of melt rate due to plume activity, although the scales used are not the same. Different scales have been chosen to account for the significant differences between the values.

lack of calving events produced by the model in that region of the glacier front that could be caused by low plume-induced melting in the area. In general, the performance of the model is better when looking just at the central 350 m of the calving front. On average, the modelled positions are 40 % closer to the observed positions when taking just this central part (13,03 m versus 20.95 m for the total front), with half of the values below 10 m. Even so, in late spring and early summer, the differences in both cases, taking the whole calving front or just the central part, are considerably small and of the same order.

Although a comparison between a 2D and a 3D model must be handled carefully, our results show a deviation of ±10 m for the central 350 m of the calving front between April and August 2010. This is the same deviation value obtained by De Andrés et al. (2018) for their flowline model. To obtain those results, they needed to include a non-dimensional adjustable parameter used to parameterize the crevasse water depths (CWD). In contrast, our model uses the 3D calving implementation of Todd et al. (2018), which ignores this process, so we do not need any CWD parameterization. Therefore, the inclusion of an across glacier dimension extends the best results of the 2D model to the central 350 m of the calving front, where the 3D model
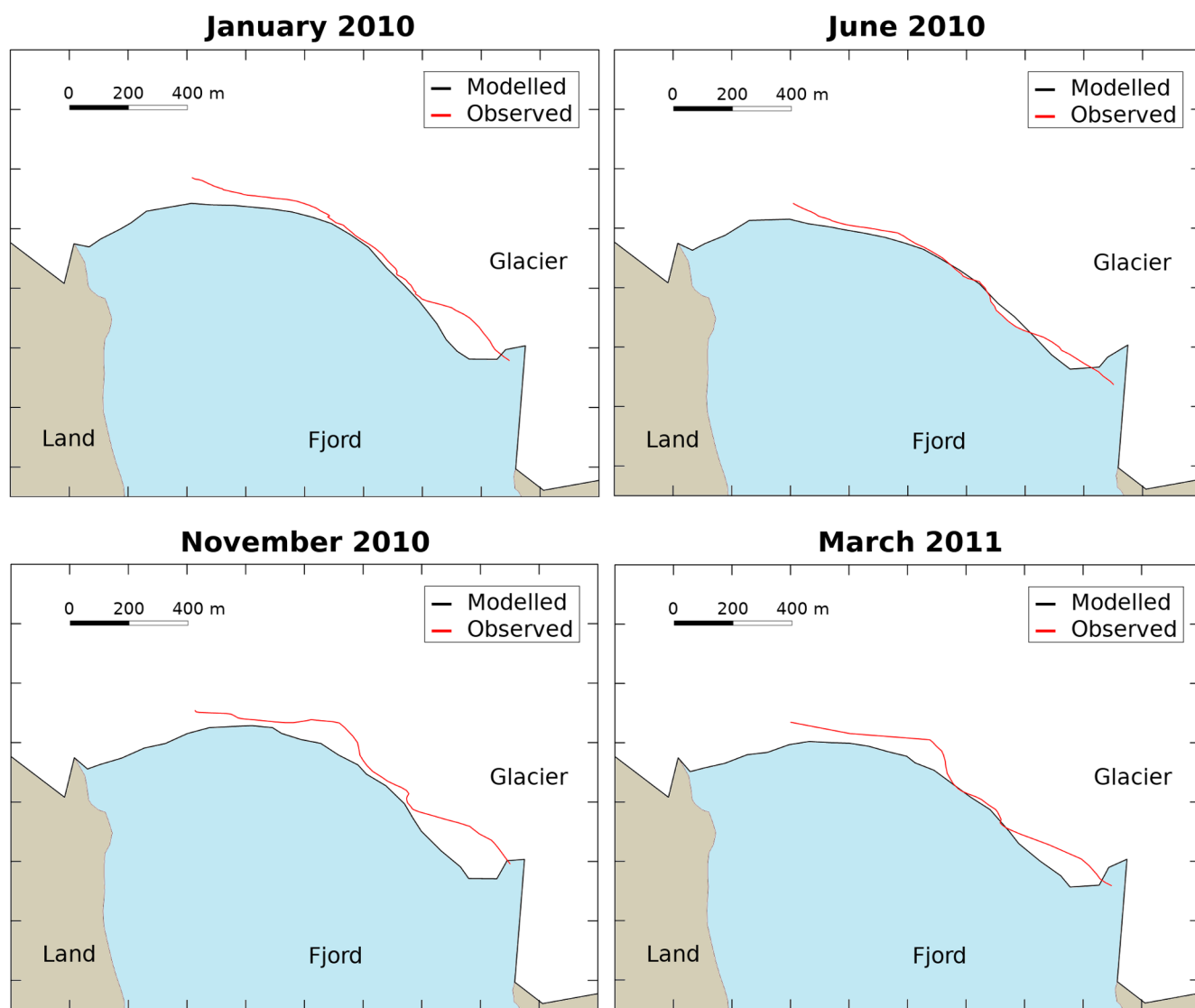
Figure 7. 2D aerial view of the glacier-fjord system for January 2010, June 2010, November 2010 and March 2011. The solid black lines represent the modelled contour of the glacier and the red lines, the observed front position. Note that the observational data do not cover the westernmost part of the front.
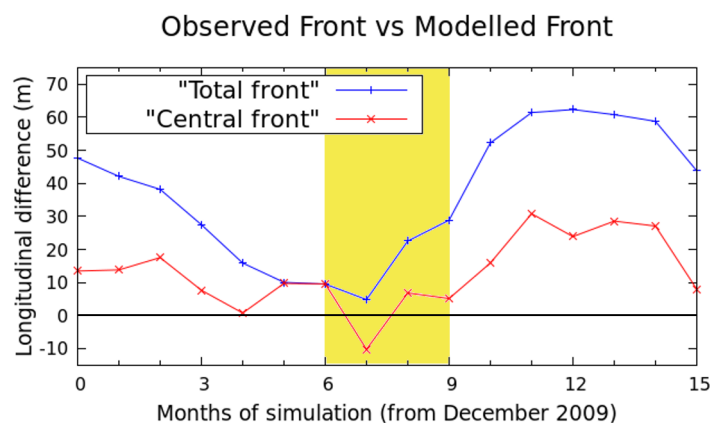
Figure 8. Evolution of the longitudinal difference between the modelled and the observed front position calculated as the difference in area between them divided by the glacier width (blue line), and that same evolution restricted to the central 350 m of the calving front (red line). Positive values indicate that the modelled front is more advanced than the observed, while negative values indicate the opposite. The zero is marked with a black horizontal line so values closer to that line indicate a better agreement between modelled and observed positions. The yellow area indicate the summer period (June to September 2010).

predicts the observed front position with a good level of agreement. However, there is a region where the modelled positions are clearly behind the observed ones. The escalation of the difference coincides with the months when calving is larger at the glacier. Consequently, the cause of this increase could be an underestimation of calving by the model. The reasons could be that the model is not able to capture all calving events occurring at the glacier or an underestimation of submarine melting, since higher values of submarine melting can enhance calving. So these two factors have to be closely examined in order to improve the performance of the model.

5   Conclusions and future work

We have developed a 3D glacier dynamics model that, in addition to solve calving and subglacial hydrology, accounts for oceanic (by a plume model) and atmospheric (by surface mass balance and surface meltwater) factors too. Subglacial hydrology provides discharge values that, in combination with appropriate fjord ambient conditions, are high enough to generate plumes at the calving front except for the coldest months, i.e., from November to April. The results for the hydrology are consistent with other studies using a similar model (Cook et al., 2020), while the results for the plume melt rate are in agreement with other works on the Hansbreen-Hansbukta glacier-fjord system (De Andrés et al., 2018).

The model is able to predict the evolution of the front position in terms of advance and retreat following a seasonal cycle with steep retreats in summer months and steady advances during the rest of the year. However, there are still differences between observed and modelled positions, specially in the eastern margin, where the longitudinal difference reaches 150 m in November 2010. In fact, when taking only the central part of the glacier front, the results improve significantly and the

modelled positions become, on average, 40 % closer to the observed ones. In general, the difference between the modelled and observed front positions increases during the calving period, and we assume that the cause is an underestimation of calving
295 by our model. Even so, the difference between the modelled and observed front positions decreases in some months, such as May, June, and July. In these months, the model is able to predict the front position with a very good level of agreement. In the eastern margin, our model is not producing enough calving events, which is causing that large differences.

Changes in SMW alone are not able to explain plumes behavior, turning fjord ambient conditions into a key factor in this process. And plume-induced melting has proven to be an essential factor for calving to occurs. Consequently, a logical next
300 step would be to use a fjord model to obtain better estimates of ambient conditions. Furthermore, the study period of this experiment is limited by the available data. Running a longer simulation could help us better understand the seasonal patterns and find out whether the eastern difference grows larger or starts to decrease at some point.

References

AMAP: Snow, Water, Ice and Permafrost in the Arctic (SWIPA), Arctic Monitoring and Assessment Programme (AMAP), Oslo, 2017.

Benn, D. I., Warren, C. R., and Mottram, R. H.: "Calving laws", "sliding laws" and the stability of tidewater glaciers, Ann. Glaciol., 46, 123–130, https://doi.org/10.3189/172756407782871161, 2007.

Benn, D. I., Cowtom, T., Todd, J., and Luckman, A.: Glacier calving in Greenland, Curr. Clim. Change Rep., 3, 282–290, https://doi.org/10.1007/s40641-017-0070-1, 2017.

Benn, D. I. and Åström, J. A.: Calving glaciers and ice shelves, Advances in Physics: X, 3, 1513 819, https://doi.org/10.1080/23746149.2018.1513819, 2018.

Bojinski, S., M.Verstraete, Peterson, T. C., Richter, C., Simmons, A., and Zemp, M.: The concept of essential climate variables in support of climate research, applications, and policy, Bulletin of the American Meteorological Society, 95, 1431–1443, https://doi.org/10.1175/BAMS-D-13-00047.1, 2014.

Błaszczyk, M., Jania, J. A., Ciepły, M., Grabiec, M., Ignatiuk, D., Kolondra, L., Kruss, A., Luks, B., Moskalik, M., Pastusiak, T., Strzelewicz, A., Walczowski, W., and Wawrzyniak, T.: Factors controlling terminus position of Hansbreen, a tidewater glacier in Svalbard, J. Geophys. Res.: Earth Surf., 126, e2020JF005 763, https://doi.org/10.1029/2020JF005763, 2021.

Cassotto, R., Fahnestock, M., Amundson, J., Truffer, M., Boettcher, M., De la Peña, S., and Howat, I.: Non-linear glacier response to calving events, Jakobshavn Isbræ, Greenland, J. Glaciol., 65, 39–54, https://doi.org/10.1017/jog.2018.90, 2018.

Church, J., Clark, P., Cazenave, A., Gregory, J., Jevrejeva, S., Levermann, A., Merrifield, M., Milne, G., Nerem, R. S., Nunn, P., Payne, A., Pfeffer, W. T., Stammer, D., and Alakkat, U.: Sea Level Change. In Stocker, T.F., D. Qin, G.-K. Plattner, M. Tignor, S.K. Allen, J. Boschung, A. Nauels, Y. Xia, V. Bex and P.M. Midgley (eds.), Climate Change 2013: The Physical Science Basis. Contribution of Working Group I to the Fifth Assessment Report of the Intergovernmental Panel on Climate Change, pp. In press. 1137–1216, 2013.

Cogley, J. G., Hock, R., Rasmussen, L. A., Arendt, A. A., Bauder, A., Braithwaite, R. J., Jansson, P., Kaser, G., Möller, M., Nicholson, L., and Zemp, M.: Glossary of glacier mass balance and related terms, IHP-VII Technical Documents in Hydrology No. 86, IACS Contribution No. 2, Paris: UNESCO-IHP., 2011.

Cook, S. J., Chrostoffersen, P., Todd, J., Slater, D., and Chaucé, N.: Coupled modelling of subglacial hydrology and calving-front melting at Store Glacier, West Greenland, The Cryosphere, 14, 905–924, https://doi.org/10.5194/tc-14-905-2020, 2020.

Cook, S. J., Chrostoffersen, P., and Todd, J.: A fully-coupled 3D model of a large Greenlandic outlet glacier with evolving subglacial hydrology, frontal plume melting and calving, J. Glaciol., 68, 486–502, https://doi.org/10.1017/jog.2021.109, 2022.

Cownton, T. R., Slater, D. A., Sole, A., Goldberg, D., and Nienow, P.: Modeling the impact of glacial runoff on fjord circulation and submarine melt rate using a new subgrid-scale parameterization for glacial plumes, J. Geophys. Res. Oceans, 120, 796–812, https://doi.org/10.1002/2014JC010324, 2015.

Cownton, T. R., Todd, J. A., and Benn, D. I.: Sensitivity of tidewater glaciers to submarine melting governed by plume locations, Geophys. Res. Lett., 46, 11 219–11 227, https://doi.org/10.1029/2019GL084215, 2019.

Cuffey, K. and Paterson, W. S. B.: The physics of glaciers, Elsevier, Oxford: Elsevier, 4th edn., 2010.

De Andrés, E., Otero, J., Navarro, F., Promińska, A., and Lapazaran, J.: A two-dimensional glacier–fjord coupled model applied to estimate submarine melt rates and front position changes of Hansbreen, Svalbard, J. Glaciol., 64, 745–758, https://doi.org/10.1017/jog.2018.61, 2018.

The Cryosphere
Discussions

Open Access
EGU

De Andrés, E., Otero, J., Navarro, F., and Walczowski, W.: Glacier–plume or glacier–fjord circulation models? A 2-D comparison for Hansbreen–Hansbukta system, Svalbard, J. Glaciol., 67, 797–810, https://doi.org/10.1017/jog.2021.27, 2021.

Edwards, T. L., Nowicki, S., Marzeion, B., Hock, R., Goelzer, H., Seroussi, H., Jourdain, N. C., Slater, D. A., Turner, F. E., Smith, C. J., McKenna, C. M., Simon, E., Abe-Ouchi, A., Gregory, J. M., Larour, E., Lipscomb, W. H., Payne, A. J., Shepherd, A., Agosta, C.,
355   Alexander, P., Albrecht, T., Anderson, B., Asay-Davis, X., Aschwanden, A., Barthel, A., Bliss, A., Calov, R., Chambers, C., Champollion, N., Choi, Y., Cullather, R., Cuzzone, J., Dumas, C., Felikson, D., Fettweis, X., Fujita, K., Galton-Fenzi, B. K., Gladstone, R., Golledge, N. R., Greve, R., Hattermann, T., Hoffman, M. J., Humbert, A., Huss, M., Huybrechts, P., Immerzeel, W., Kleiner, T., Kraaijenbrink, P., Le clec'h, S., Lee, V., Leguy, G. R., Little, C. M., Lowry, D. P., abd D. F. Martin, J. M., Da Maussion, F., Morlighem, M., O'Neill, J. F., Nias, I., Pattyn, F., Pelle, T., Price, S. F., Quiquet, A., Radić, V., Reese, R., Rounce, D. R., Rückamp, M., Sakai, A., Shafer, C.,
360   Schlegel, N., Shannon, S., abd F. Straneo, R. S. S., Sun, S., Tarasov, L., Trusel, L. D., Van Breedam, J., van de Wal, R., van den Broeke, M., Winkelmann, R., Zekollari, H., Zhao, C., Zhang, T., and Zwinger, T.: Projected land ice contributions to twenty-first-century sea level rise, Nature, 593, 74–82, https://doi.org/10.1038/s41586-021-03302-y, 2021.

Finkelnburg, R.: Climate variability of Svalbard in the first decade of the 21st century and its impact on Vestfonna ice cap, Nordaustlandet, Doctoral Thesis, Technischen Universität Berlin, https://doi.org/10.14279/depositonce-3598, 2013.

365   Fried, M. J., Catania, G. A., Bartholomaus, T. C., Duncan, D., Davis, M., Stearns, L. A., Nahs, J., Shroyer, E., and Sutherland, D.: Distributed subglacial discharge drives significant submarine melt at a Greenland tidewater glacier, Geophys. Res. Lett., 42, 9328–9336, https://doi.org/10.1002/2015GL065806, 2015.

Gagliardini, O. and Werder, M.: Influence of increasing surface melt over decadal timescales on land-terminating Greenland-type outlet glaciers, J. Glaciol., 64, 700–710, https://doi.org/10.1017/jog.2018.59, 2018.

370   Gagliardini, O., Zwinger, T., Gillet-Chaulet, F., Durand, G., Favier, L., de Fleurian, B., Greve, R., Malinen, M., Martín, C., Råback, P., Ruokolainen, J., Sacchettini, M., Schäfer, M., Seddik, H., and Thies, J.: Capabilities and performance of Elmer/Ice, a new-generation ice sheet model, Geoscientific Model Development, 6, 1299–1318, https://doi.org/10.5194/gmd-6-1299-2013, 2013.

Gillet-Chaulet, F., Gagliardini, O., Seddik, H., Nodet, M., Durand, G., Ritz, C., Zwinger, T., Greve, R., and Vaughan, D. G.: Greenland ice sheet contribution to sea-level rise from a new-generation ice-sheet model, The Cryosphere, 6, 1561– 1576, https://doi.org/10.5194/tc-6-
375   1561-2012, 2012.

Grabiec, M., Jania, J. A., Puczko, D., Kolondra, L., and Budzik, T.: Surface and bed morphology of Hansbreen, a tidewater glacier in Spitsbergen, Polish Polar Research, 33, 111–138, https://doi.org/10.2478/v10183-012-0010-7, 2012.

Hanna, E., Pattyn, F., Navarro, F., Favier, V., Goelzer, H., van den Broeke, M. R., Vizcaino, M., Whitehouse, P. L., Ritz, C., Bulthuis, K., and Smith, B.: Mass balance of the ice sheets and glaciers–progress since AR5 and challenges, Earth-Science Reviews, 201, 102 976,
380   https://doi.org/10.1016/j.earscirev.2019.102976, 2020.

Hewitt, I. J.: Subglacial plumes, Annual Review of Fluid Mechanics, 52, 145–169, https://doi.org/10.1146/annurev-fluid-010719-060252, 2020.

Hock, R., Bliss, A., Marzeion, B., Giesen, R. H., Hirabayashi, Y., Huss, M., Radić, V., and Slangen, A. B. A.: GlacierMIP – A model intercomparison of global-scale glacier mass-balance models and projections, J. Glaciol., 65, 453–467, https://doi.org/10.1017/jog.2019.22,
385   2019.

Holmes, F. A., Kirchner, N., Kuttenkeuler, J., Krützfeldt, J., and Noormets, R.: Relating ocean temperatures to frontal ablation rates at Svalbard tidewater glaciers: Insights from glacier proximal datasets, Sci. Rep., 9, 9442, https://doi.org/https://doi.org/10.1038/s41598-019-45077-3, 2019.

Hugonnet, R., McNabb, R., Berthier, E., Menounos, B., Nuth, C., Girod, L., Farinotti, D., Huss, M., Dussaillant, I., Brun, F., and Kääb, A.:
Accelerated global glacier mass loss in the early twenty-first century, Nature, 592, 726–731, https://doi.org/10.1038/s41586-021-03436-z,
2021.

Huss, M. and Hock, R.: A new model for global glacier change and sea-level rise, Front. Earth Sci., 3, 1–22,
https://doi.org/10.3389/feart.2015.00054, 2015.

IPCC: IPCC Climate Change 2021: The Physical Science Basis. Contribution of Working Group I to the Sixth Assessment Re-
port of the Intergovernmental Panel on Climate Change, Cambridge University Press, Cambridge, UK and New York, NY, USA,
https://doi.org/10.1017/9781009157896, 2021.

Isaksen, K., Nordli, Ø., Førland, E. J., Łupikasza, E., Eastwood, S., and Niedźwiedź, T.: Recent warming on Spitsbergen – influence of
atmospheric circulation and sea ice cover, J. Geophys. Res. Atmos., 121, 11 913–11 931, https://doi.org/10.1002/2016JD025606, 2016.

Jackson, R. H., Shroyer, E. L., Nash, J. D., Sutherland, D. A., Carroll, D., Fried, M. J., Catania, G. A., Bartholomaus, T. C., and Stearns, L. A.:
Near-glacier surveying of a subglacial discharge plume: implications for plume parameterizations, Geophys. Res. Lett., 44, 6886–6894,
https://doi.org/10.1002/2017GL073602, 2017.

Jackson, R. H., Nash, J. D., Kienholz, C., Sutherland, D. A., Amundson, J. M., Motyka, R. J., Winters, D., Skyllingstad, E., and Pettit,
E. C.: Meltwater intrusions reveal mechanisms for rapid submarine melt at a tidewater glacier, Geophys. Res. Lett., 47, e2019GL085 335,
https://doi.org/10.1029/2019GL085335, 2019.

Jenkins, A.: A one-dimensional model of ice shelf-ocean interaction, J. Geophys. Res., 96, 671–677, 1991.

Jenkins, A.: Convection-driven melting near the grounding lines of ice shelves and tidewater glaciers, J. Phys. Oceanogr., 41, 2279–2294,
https://doi.org/10.1175/JPO-D-11-03.1, 2011.

Jouvet, G., Weidmann, Y., Kneib, M., Detert, M., Seguinot, J., Sakakibara, D., and Sugiyama, S.: Short-lived ice speed-up and plume water
flow captured by a VTOL UAV give insights into subglacial hydrological system of Bowdoin Glacier, Remote Sens. Environ., 17, 389–399,
https://doi.org/10.1016/j.rse.2018.08.027, 2018.

Kochtitzky, W., Copland, L., Van Wychen, W., Hugonnet, R., Hock, R., Dowdeswell, J. A., Benham, T., Strozzi, T., Glazovsky, A., Lavrentiev,
I., Rounce, D. R., Millan, R., Cook, A., Dalton, A., Jiskoot, H., Cooley, J., Jania, J., and Navarro, F.: The unquantified mass loss of Northern
Hemisphere marine-terminating glaciers from 2000–2020, Nat. Commun., 13, 5835, https://doi.org/10.1038/s41467-022-33231-x, 2022.

Luckman, A., Benn, D. I., Cottier, F., Bevan, S., Nilsen, F., and Inall, M.: Calving rates at tidewater glaciers vary strongly with ocean
temperature, Nat. Commun., 6, 8566, https://doi.org/10.1038/ncomms9566, 2015.

Meier, M. F., , Dyurgerov, M. B., Rick, U. K., O'neel, S., Pfeffer, W. T., Anderson, R. S., Anderson, S. P., and Glazovsky, A. F.: Glaciers
dominate eustatic sea-level rise in the 21st century, Science, 317, 1064, https://doi.org/10.1126/science.1143906, 2007.

Morton, B. R., Taylor, G., and Turner, J. S.: Turbulent gravitational convection from maintained and instantaneous sources, Proceedings of
the Royal Society A: Mathematical, Physical and Engineering Sciences, 234, 1–23, https://doi.org/10.1098/rspa.1956.0011, 1956.

Motyka, R. J., Dryer, W. P., Amundson, J., Truffer, M., and Fahnestock, M.: Rapid submarine melting driven by subglacial discharge, LeConte
Glacier, Alaska, Geophys. Res. Lett., 40, 5153–5158, https://doi.org/10.1002/grl.51011, 2013.

Möller, M., Navarro, F., Huss, M., and Marzeion, B.: Projected sea-level contributions from tidewater glaciers are highly sensitive to chosen
bedrock topography: A case study at Hansbreen, Svalbard, J. Glaciol., p. 1–15, https://doi.org/10.1017/jog.2022.117, 2023.

Navarro, F. J., Martín-Español, A., Lapazaran, J. J., Grabiec, M., Otero, J., Vasilenko, E. V., and Puczko, D.: Ice volume esti-
mates from Ground-Penetrating Radar surveys, Wedel Jarlsberg Land Glaciers, Svalbard, Arct. Antarct. Alp. Res., 46, 394–406,
https://doi.org/10.1657/1938-4246-46.2.394, 2014.

Nick, F. M., Van der Veen, C., Vieli, A., and Benn, D. I.: A physically based calving model applied to marine outlet glaciers and implications for the glacier dynamics, J. Glaciol., 56, 781–794, https://doi.org/10.3189/002214310794457344, 2010.

Nordli, Ø., Wyszyński, P., Gjelten, H. M., Isaksen, K., Łupikasza, E., Niedźwiedź, T., and Przybylak, R.: Revisiting the extended Svalbard Airport monthly temperature series, and the compiled corresponding daily series 1898–2018, Polar Res., 39, https://doi.org/10.33265/polar.v39.3614, 2020.

Oerlemans, J., Jania, J., and Kolondra, L.: Application of a minimal glacier model to Hansbreen, Svalbard, The Cryosphere, 5, 1–11, https://doi.org/10.5194/tc-5-1-2011, 2011.

Otero, J., Navarro, F. J., Martin, C., Cuadrado, M. L., and Corcuera, M.: A three-dimensional calving model: numerical experiments on Johnsons Glacier, Livingston Island, Antarctica, J. Glaciol., 56, 200–214, https://doi.org/10.3189/002214310791968539, 2010.

Otero, J., Navarro, F. J., Lapazaran, J. J., Welty, E., Puczko, D., and Finkelnburg, R.: Modeling the controls on the front position of a tidewater glacier in Svalbard, Front. Earth Sci., 5, https://doi.org/10.3389/feart.2017.00029, 2017.

Perez-Doña, I. and Otero, J.: Sobre el uso de Kriging Bayesiano para estimar la evolución de las velocidades en superficie del Glaciar Hansbreen (Svalbard), 10a Asamblea Hispano-Portuguesa de Geodesia y Geofísica, In Press, 2023.

Pętlicki, M., Ciepły, M., Jania, J., Promińska, A., and Kinnard, C.: Calving of a tidewater glacier driven by melting at the waterline, J. Glaciol., 61, 851–863, https://doi.org/10.3189/2015JoG15J062, 2015.

Rignot, E., Koppes, M., and Velicogna, I.: Rapid submarine melting of the calving faces of west Greenland glacier, Nature Geoscience, 3, 187–191, https://doi.org/10.1038/ngeo765, 2010.

Slater, D. A., Nienow, P., Cownton, T. R., Goldberg, D., and Sole, A.: Effect of near-terminus subglacial hydrology on tidewater glacier submarine melt rates, Geophys. Res. Lett., 42, 2861–2868, https://doi.org/10.1002/2014GL062494, 2015.

Slater, D. A., Straneo, F., Das, S. B., Richards, C. G., Wagner, T. J. W., and Nienow, P. W.: Localized plumes drive front-wide ocean melting of a Greenlandic tidewater glacier, Geophys. Res. Lett., 45, 12 350–12 358, https://doi.org/10.1029/2018GL080763, 2018.

Straneo, F. and Cenedese, C.: The dynamics of Greenland's glacial fjords and their role in climate, Annu. Rev. Mar. Sci, 7, 89–112, https://doi.org/10.1146/annurev-marine-010213-135133, 2015.

Sutherland, D. A., Jackson, R. H., Kienholz, C., Amundson, J. M., Dryer, W. P., Duncan, D., Eidam, E. F., Motyka, R. J., and Nash, J. D.: Direct observations of submarine melt and subsurface geometry at a tidewater glacier, Science, 365, 369–374, https://doi.org/10.1126/science.aax3528, 2019.

Todd, J. and Christoffersen, P.: Are seasonal calving dynamics forced by buttressing from ice mélange or undercutting by melting? Outcomes from full-Stokes simulations of Store Glacier, West Greenland, The Cryosphere, 8, 2353–2365, https://doi.org/10.5194/tc-8-2353-2014, 2014.

Todd, J., Christoffersen, P., Zwinger, T., Råback, P., Chauché, N., Benn, D., Luckman, A., Ryan, J., Toberg, N., Slater, D., and Hubbard, A.: A full-Stokes 3D calving model applied to a large greenlandic glacier, J. Geophys. Res.: Earth Surf., 123, 410–432, https://doi.org/10.1002/2017JF004349, 2018.

Todd, J., Christoffersen, P., Zwinger, T., Râback, P., and Benn, D. I.: Sensitivity of a calving glacier to ice–ocean interactions under climate change: new insights from a 3-D full-Stokes model, The Cryosphere, 13, 1681–1694, https://doi.org/10.5194/tc-13-1681-2019, 2019.

Vallot, D., Adinugroho, S., Strand, R., How, P., Pettersson, R., Benn, D. I., and Hulton, N. R. J.: Automatic detection of calving events from time-lapse imagery at Tunabreen, Svalbard, Geosci. Instrum. Method. Data Syst., 8, 113–127, https://doi.org/10.5194/gi-8-113-2019, 2019.

Vieli, A., Funk, M., and Blatter, H.: Tidewater glaciers: Frontal flow acceleration and basal sliding, Ann. Glaciol., 31, 217–221,

465   https://doi.org/10.3189/172756400781820417, 2000.

Vieli, A., Jania, J., and Kolondra, L.: The retreat of a tidewater glacier: Observations and model calculations on Hansbreen, Spitsbergen,

J. Glaciol., 48, 592–600, https://doi.org/10.3189/172756502781831089, 2002.

Werder, M. A., Hewitt, I. J., Schoof, C. G., and Flowers, G. E.: Modeling channelized and distributed subglacial drainage in two dimensions,

J. Geophys. Res.: Earth Surf., 118, 21402 158, https://doi.org/10.1002/jgrf.20146, 2013.

470   Xie, S., Dixon, T. H., Holland, D. M., Voytenko, D., and Vaňková, I.: Rapid iceberg calving following removal of tightly packed pro-glacial

mélange, Nat. Commun., 10, 3250, https://doi.org/10.1038/s41467-019-10908-4, 2019.